Repair wind field in oil contaminated areas with SAR images*

GUO Jie (过杰)[1, **], HE Yijun (何宜军)[2, 3], LONG Xiao (隆霄)[4], HOU Chawei (侯查伟)[5],
LIU Xin (刘欣)[1], MENG Junmin (孟俊敏)[6, **]

[1] *Yantai Institute of Coastal Zone Research, Chinese Academy of Sciences; Key Laboratory of Coastal Zone Environmental Processes and Ecological Remediation, CAS, Yantai 264003, China*

[2] *School of Marine Sciences, Nanjing University of Information Science & Technology, Nanjing 210044, China*

[3] *Key Laboratory of Ocean Circulation and Waves, Institute of Oceanology, Chinese Academy of Science, Qingdao 266071, China*

[4] *Key Laboratory of Arid Climate Change and Reducing Disaster of Gansu Province, College of Atmospheric Sciences, Lanzhou University, Lanzhou 730000, China*

[5] *Yantai Marine Environmental Monitoring Central Station, State Oceanic Administration (SOA), Yantai 264006, China*

[6] *First Institute of Oceanography, State Oceanic Administration (SOA), Qingdao 266061, China*

Abstract   In this paper, we compared the normalized radar cross section in the cases of oil spill, biogenic slicks, and clean sea areas with image samples made from 11-pixel NRCS average, and determined their thresholds of the NRCS of the synthetic aperture radar. The results show that the thresholds of oil and biogenic slicks exhibit good consistency with the corresponding synthetic aperture radar images. In addition, we used the normalized radar cross section of clean water from adjacent patches of oil or biogenic slicks areas to replace that of oil or biogenic slicks areas, and retrieve wind field by CMOD5.n and compare wind velocity mending of oil and biogenic slicks areas with Weather Research and Forecasting modeled data, from which the root mean squares of wind speed (wind direction) inversion are 0.89 m/s (20.26°) and 0.88 m/s (7.07°), respectively. Therefore, after the occurrence of oil spill or biogenic slicks, the real wind field could be repaired using the method we introduced in this paper. We believe that this method could improve the accuracy in assessment of a real wind field on medium and small scales at sea, and enhance effectively the monitoring works on similar oil or biogenic slicks incidents at sea surface.

Keyword: wind speed; oil spill; biogenic slicks; normalized radar cross section

1 INTRODUCTION

A wind vector of sea surface is a physical parameter important for understanding atmospheric dynamics, air-sea interactions, and climate. Synthetic aperture radar (SAR) is an active microwave sensor that works all-weather day-and-night in high spatial resolution, which makes it essential for wind velocity inversion, and for monitoring oil spills, biogenic slicks etc. The sea surface roughness responsible for SAR backscatter is produced primarily by capillary and small gravity waves generated by local winds (Brekke and Solberg, 2005). The damping of these waves by oil spills and biogenic slicks appears as dark features on the SAR image (Brekke and Solberg, 2005). The occurrence of an oil spill and biogenic slicks affects the normalized radar cross section (NRCS) of SAR, which would lead to a decrease in precision of the wind field retrieval. However, oil spill and biogenic slicks detection in SAR images is not an easy task. Other physical phenomena can also generate dark areas and SAR images are affected by multiplicative noise known as speckle (Brekke and Solberg, 2005). Dark areas not related to oil spills are said to be look-alike. Phenomena that give rise to the look-alike include biogenic films, low-wind areas, areas of wind-shadow near coasts, rain cells, currents, upwelling zones, internal waves, and oceanic or

** Corresponding authors: jguo@yic.ac.cn; mengjm@fio.org.cn

Table 1 Data specification

Data name	Time	Polarization mode	Spatial resolution	Band of sensor	Watch width
ENVISAT-ASAR-WSM	2011-06-11	VV	150×150 m	C	>400 km
ENVISAT-ASAR-IMM	2011-07-20	VV	30×30m	C	Up to 100 km

atmospheric fronts (Brekke and Solberg, 2005).

Oil spill detection in SAR image can be divided into three phases. They are dark area detection (Solberg and Theophilopoulos, 1997; Espedal and Wahl, 1999; Del Frate et al., 2000; Espedal and Johannessen, 2000; Fiscella et al., 2000; Topouzelis et al., 2003), features extraction (Solberg et al., 1999; Brekke and Solberg, 2005; Keramitsoglou et al., 2005; Karathanassi et al., 2006), and oil spill/look-alike classification (Del Frate et al., 2000; Fiscella et al., 2000; Keramitsoglou et al., 2006; Topouzelis et al., 2009). Dark area detection algorithms are based generally on filtering techniques accomplished on multi-look single-polarization SAR data (Migliaccio et al., 2009).

Ocean surface wind retrieval from conventional single-polarization SAR backscatter measurements is achieved by using various geophysical model functions (GMFs) for X-, C-, and L-band SAR. Specifically, for C-band, the commonly used GMFs are CMOD4 (Stoffelen and Anderson, 1997), CMOD_IFR2 (Quilfen et al., 1998), and CMOD5.n (Hersbach, 2010). Single-frequency (C- or L-band) and single-polarization (VV or HH) SAR systems, such as ENVISAT ASAR (advanced synthetic aperture radar) and COSMO data, have been used to retrieve ocean surface wind speeds with various GMFs and polarization radio (PR) models (Zhang et al., 2012). In this paper, wind fields are retrieved from ASAR data by CMOD5.n by marking oil spill or biogenic slicks areas, through backscatter coefficient weighted average of the adjacent clean sea area make up the oil spill or biogenic slicks areas. This work could improve the accuracy of assessment to a real wind field to medium and small scales (Feng et al., 2003) and provide data support for identification and monitoring of disastrous events such as oil spills or biogenic slicks areas in maritime.

2 DATA AND METHOD

2.1 Data and study area

Two modes of ENVISAT-ASAR data are used in this study: wide swath mode (WSM) and image mode (IM) (Table 1). We analyzed the influence of oil spill and biogenic slicks on the NRCS, and wind velocity

inversion with ENVISAT ASAR data in CMOD5.n.

ENVISAT satellite is one of a series of the Earth observation satellite launched on March 1, 2002, the largest environmental satellite of the Europe with 10 instruments aboard and at eight tons. ASAR is the heaviest instruments on the ENVISAT satellite. The ASAR was able to generate high-resolution images on various areas, such as ocean, coastal zone, polar ice caps, and land, with which changes in the oceans can be studied. As a continuation of ERS-1/2 SAR satellite, Envisat-1 was used specifically to continuously monitor the Earth's environments at the surface and in the atmosphere for geo-mapping, resource exploration, weather broadcast, and disaster warning. After her commission for 10 years, the satellite lost communication with the Earth on 8 April 2012. Featured with high resolution, the Envisat-ASAR data could catch the incidence of oil spill on its track. Therefore, SAR plays an important role in recording marine disaster events, such as oil spill.

The case area for oil spill was in the Bohai Sea (37°–42°N, 117°–121°E) (Guo et al., 2013) and that for biogenic slicks was in the East China Sea (27.6°–29.9°N, 124.3°–125.7°E) (Fig.1). We compared the changes caused by oil spill and biogenic slicks on the NRCS using ENVISAT ASAR data, which can be used to analyze the effects of oil spill and biogenic slicks on the retrieval of wind speed data. The data for wind field inversion were the Advanced Scaterometer (ASCAT) data; and the Weather Research and Forecasting (WRF) model was deployed as the auxiliary.

The ASCAT is one of the instruments that carried on-board Meteorological Operational (MetOp) polar satellites launched by the European Space Agency (ESR) and operated by the European organization for the exploitation of Meteorological Satellites (EUMETSAT). ASCAT was launched on 19 October 2006 in C band in frequency at 5.255 GHz. The wind products of ASCAT are distributed in two resolutions at 50 km in 25-km grid and at 25 km in 12.5-km grid. Both are available as regional EUMETSAT Advanced Retransmission Service (EARS) products in ~30 interval of sensing and as global OSISAF products in
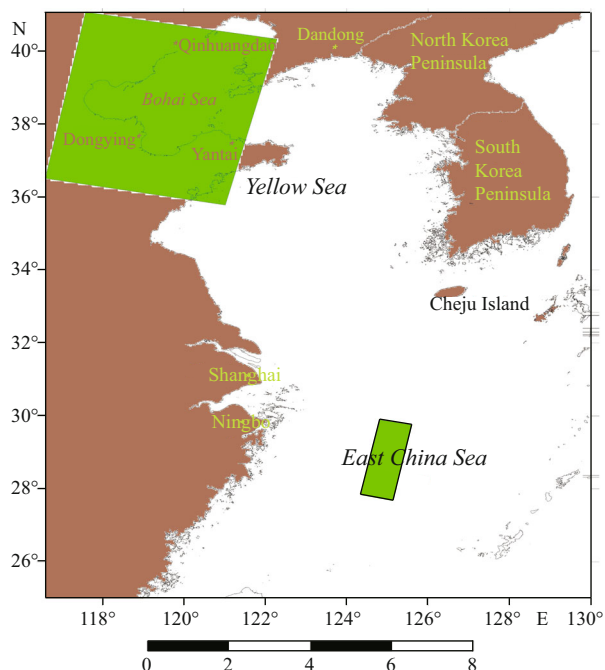
Fig.1 Case study areas: oil-spill area in Bohai Sea (the upper rectangular); biogenic slicks area in East China Sea (the lower rectangular)

sensing frequency of 2.5–3 h. In this paper, the 25-km daily resolution product in 12.5-km grid data (daily average) was used.

The wind data used are the output of the WRF model with Advanced Research WRF (ARW) in dynamic core version 3.3.1 (Skamarock and Klemp, 2008). WRF is a mesoscale non-hydrostatic modeling system to a limited-area, and could do terrain tracking, which can be used for simulations from a large-eddy to a global scale.

The latest C-band geophysical model function (GMF) CMOD5 was developed by European Centre for Medium-Range Weather Forecasts (ECMWF) and KNMI for use with the ERS and ASCAT scatterometers. It has been developed using advanced empirical methods, ECMWF model winds that tied to buoy measurement data, and measurements in extreme wind conditions (e.g., hurricanes) from the unique Imaging Wind and Rain Airborne Profiler (IWRAP) instrument aircraft campaigns.

2.2 SAR image samples analysis

2.2.1 Method

We used ENVISAT ASAR data to detect oil spills and biogenic slicks. Several image-processing techniques were used, including calibration and re-

projection (Figs.2 and 3).

The wind fields retrieved by ASCAT data in the oil spill region is shown in Fig.4 and that of biogenic slick region in Fig.5. We found that the wind speeds in these two regions were below 9 m/s and the incident angles of the ROI were within 30°. Therefore, it is capable of discriminating between different surface films with SAR data (Gade and Alpers, 1998). We selected 10 image samples (11-pixel NRCS-averaged as one sample for noise elimination) from the following areas: oil-spill area (the biogenic slicks), and clean-sea (nearby oil spill area: the incident angle less than 1° area).

2.2.2 Analysis results

Figure 6a shows that the average NRCS of oil spill (data1) is -20.48 dB, and that of clean sea (data2) is -12.35 dB. The average NRCS of data1 was 8.13 dB, which is smaller than the average of data2.

The average NRCS of data1 (biogenic slicks) is -22.97 dB and the average NRCS of data2 (clean sea) is -15.76 dB. The average NRCS of data1 is 8.20 dB, which is lower than the average of data2 in Fig.6b.

Therefore, oil spill and biogenic slicks could dampen capillary gravity waves and lead to the decreases in NRCS of SAR. Non-Bragg scattering is the dominating mechanism in the areas that covered by oil spill or biogenic slick (Fig.6a, b).

2.3 Threshold determination

Several image-processing techniques were used (Figs.7a and 8a), including calibration, re-projection, mean-value filtration (3×3), and Gama filtration (3×3). Calibration is to get the image of each pixel of NRCS, and then to remove the influence of the incident angle. Re-projection is to remove the mirror effect. Mean-value filtration is to keep the original information of image as much as possible to smooth the image appropriately. Gamma filtration can keep the information at the edge and reduce the speckle noise at the same time (Han et al., 2013). In this study, the adaptive threshold was applied. We determined the mean values of the accident area (oil spill or biogenic slicks area). Figures 7b and 8b show the images of oil spill (the adaptive threshold: -15.90 dB) and biogenic slicks (the adaptive threshold: -17.27 dB) extracted through the threshold values of NRCS.

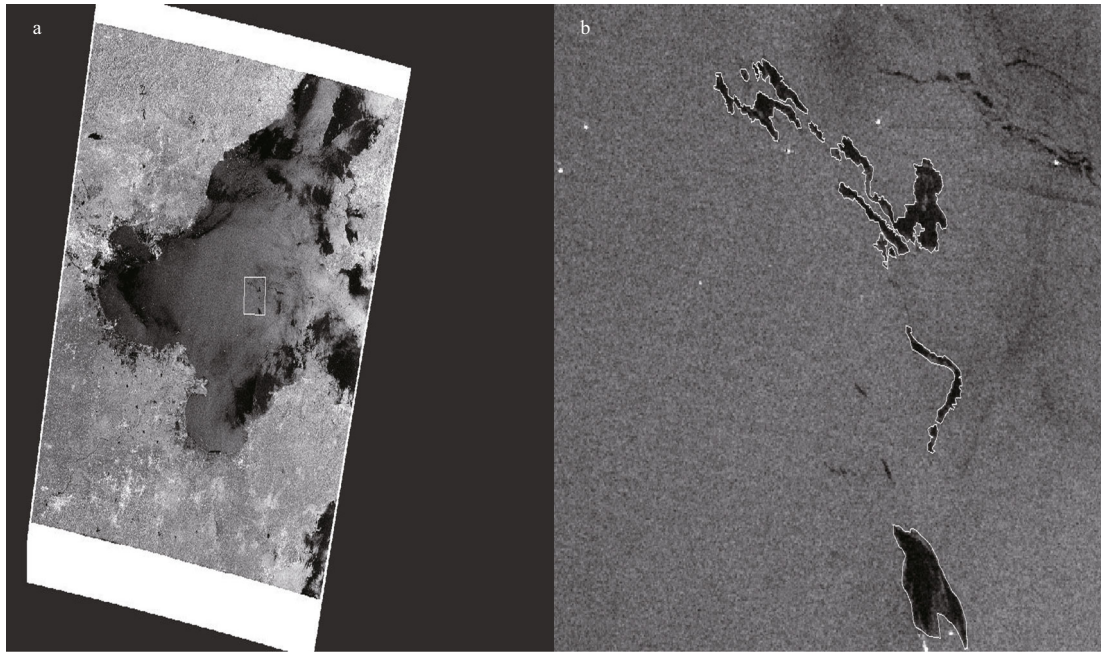Therefore, how to repair the wind field in these areas has become an issue of this study. Although the

Fig.2 The oil spill case is in the Bohai Sea on June 11, 2011

a. area of the rectangular in upper-left corner of Fig.1; b. regions of interest (ROI) is the enlarged area of the small square in Fig.2a. Black patches indicate oil spill patches.
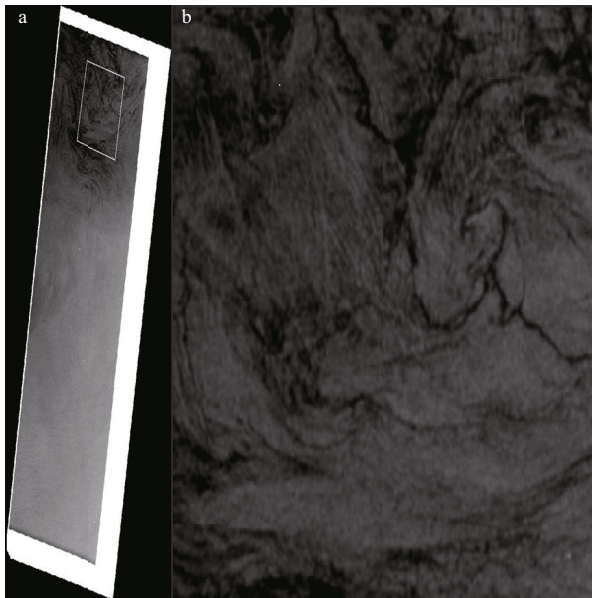

Fig.3 The case of biogenic slicks in the East China Sea on July 20, 2011

a: the area of the rectangular in lower-right of Fig.1; b. ROI: the enlarge area of the small square in Fig.3a. Black floccules are biogenic slick.

impact can be negligible for wind field inversion in small scale oil spill or biogenic slick cases for a low-resolution scatterometer, but small and meso-scale such cases can have a significant impact on local wind field inversion for a high-resolution SAR and scatterometer.
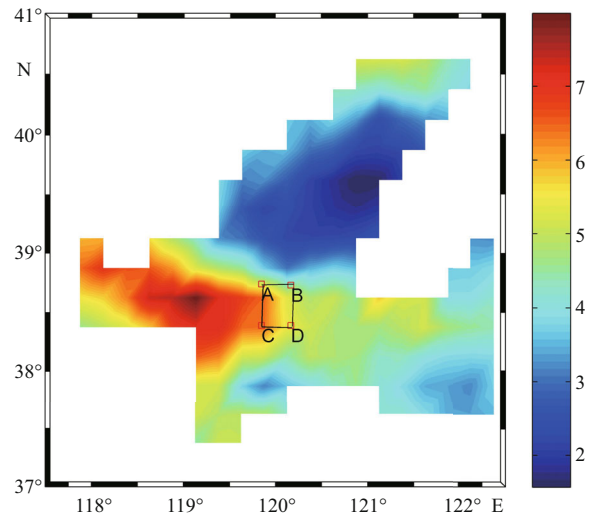

Fig.4 Wind speed retrieved by ASCAT data in oil-spill area of the Bohai Sea on June 11, 2011

3 DISCUSSION

3.1 Wind field repair

In this section, we study wind field repair in oil spill and biogenic slicks areas by CMOD5.n as shown in Figs.2a and 3a (rectangular areas).

First, radiation on SAR data is calibrated, in which the pixels average of image size for wind speed and direction retrievals is 80×80 at resolution 6×6 km for WSM data and 1×1 km for IM data (rectangle ABDC

repaired area of Figs.9a, 10a).

Second, the wind vectors of the oil spill and biogenic slicks regions are retrieved and repaired. Wind speed inversion is conducted with CMOD5.n, in which the maximum wind velocity for inversion was set to 10 m/s. The initial input of wind field of the Bohai Sea is from buoy data that deployed at 38°2′1.68″N/119°51′3.6″E on June 11, 2011. Average wind speed at 10 AM was 4.1 m/s and average wind direction was 337°; while the wind field data of the East China Sea are from ASCAT at 28°37′30″N/125°7′30″E on July 20, 2011, daily average was used to reduce the impact of biological slick on NRCS, wind speed 7.26 m/s, and average wind direction 66.218°.

Finally, the NRCS-weighted average of adjacent clear-sea areas nearby oil spill scene is used for mending the NRCS of oil spill and biogenic slick areas. The maximum threshold for oil spill is -9.94 dB, and biogenic slicks for -10.4 dB; while the averages of the clean-sea areas around the two incident scenes are -9.64 and -9.89 dB, respectively. The retrieved wind vectors are presented in Figs.9a and 10a, corresponding to the regions shown in Figs.2b and 3b, respectively.

If the threshold of scattering coefficient is smaller than the minimum of the clean-sea water, the average of the clean-sea areas is used to replace those of the scenes. In this study, the average for oil spill scene was -9.64 dB, and -9.89 dB for biogenic slicks as mentioned in the last paragraph. In addition, Rectangle ABDC in Fig.9 (38.33°–38.65°N, 119.87°–120.10°E) is the ROI of the oil spill area (11.33 km^2) and Rectangle ABDC in Fig.10 (28.961 6°–29.898°N, 124.638 1°–125.597 9°E) is the ROI of biogenic slick area (24.22 km^2).
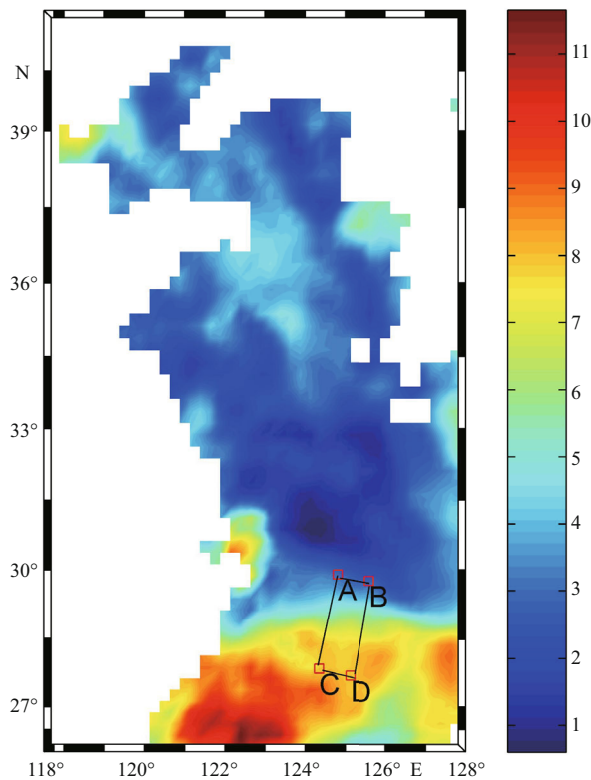
3.2 Verification on the wind field repaired

As the ASCAT itself contains the signal of oil contamination, we used WRF model to validate the wind field repaired.

The configuration of Weather Research and Forecasting (WRF) Model in this study is shown in Table 2. The initial field and lateral boundary condition were come from the USA National Centers

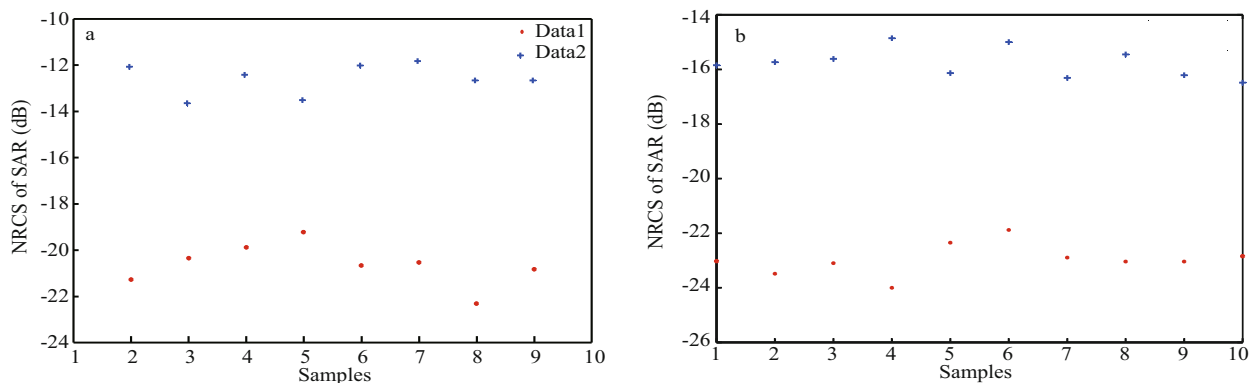**Fig.5 Wind speed retrieval by ASCAT data in biogenic slicks area of East China Sea on July 20, 2011**

Fig.6 Comparison of the NRCS of SAR between oil-spill (biological slick) and clean-sea areas on June 11, 2011 (July 20, 2011) in the Bohai Sea (the East China Sea)

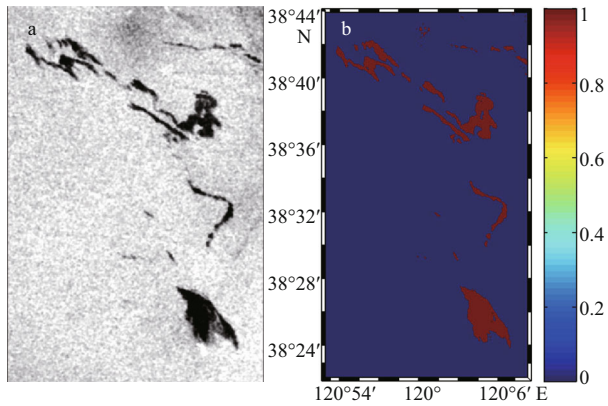Data1: average NRCS of oil spill (biogenic slicks) samples; data2: average NRCS of clean-sea samples.

Fig.7 Oil spill distribution section in the Bohai Sea on June 11, 2011 in Fig.2b

a. ROI; b. extracted oil film according to the threshold values.
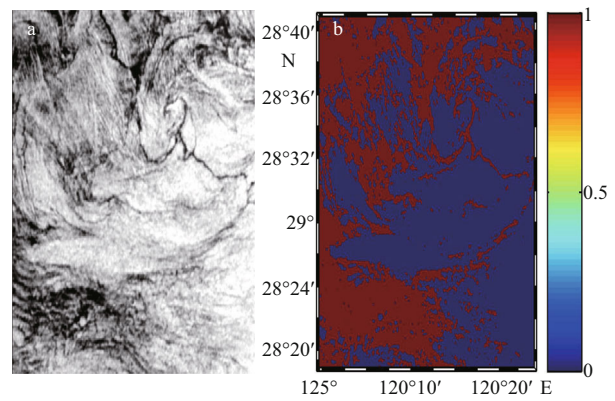

Fig.8 Biogenic slicks distribution section in the East China Sea on July 20, 2011 from Fig.3b

a. ROI; b. extracted biogenic slicks according to the threshold values.

for Environmental Prediction (NCEP) FNL (Final) Operational Global Analysis; and they are on 1°×1° grid in time interval of six hours.

The result shows that the difference of wind vector between ASAR retrieved and WRF simulated is within 0.1° and the temporal difference is less than 30 min.

Figure 11 shows the wind field simulation by WRF model on the spilled oil scene at 10 AM on June 11, 2011 in the Bohai Sea (rectangular ABDC). We used the simulation result to verify the repaired wind field data of the oil spill scene. In this area, 39 pairs of wind speed and wind direction were compared for the ROI in Fig.9b with those in Fig.11. The RMS, A-error and R-error in wind speed (wind direction) are 0.89 m/s (20.26°), 0.74 m/s (19.94°), and -0.02 m/s

(-0.11°), respectively (Table 3), which is a very good result (Fig.12a, b).

In addition, as shown in Fig.13a, a depression on the west side of the study area (biological slicks) in the East China Sea would affect the wind field repair additional to the biological slick incidence. Therefore, to repair the wind field, one shall consider the impact of depression.

Based on the result that repaired biogenic slicks, we must as well to repair the NRCS of low wind zone, for which we used the NRCS of corresponding wind area (e.g. Fig.13b) to make the repair, and then applied CMOD5.n to retrieve the wind field (Fig.10b). In this practice, 172 pairs of data were used for comparison between ASAR data and simulated ones. The results
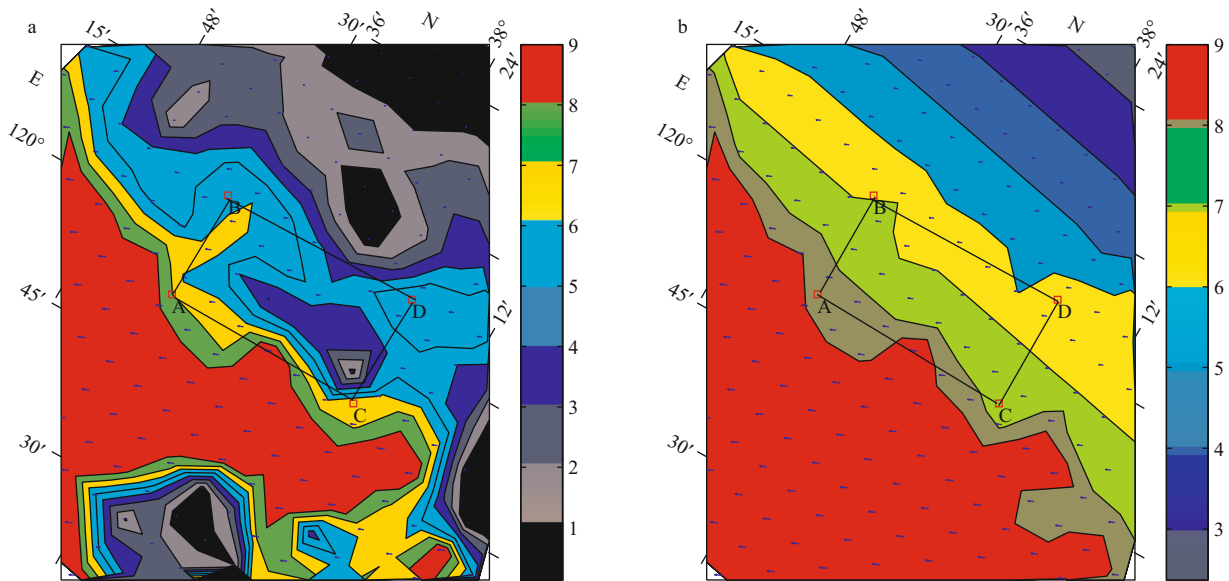

Fig.9 ASAR retrieved wind vectors at sea surface in the oil spill area in the Bohai Sea on June 11, 2011

a. wind field retrieved; b. wind field repaired (rectangle ABDC in Fig.2b).
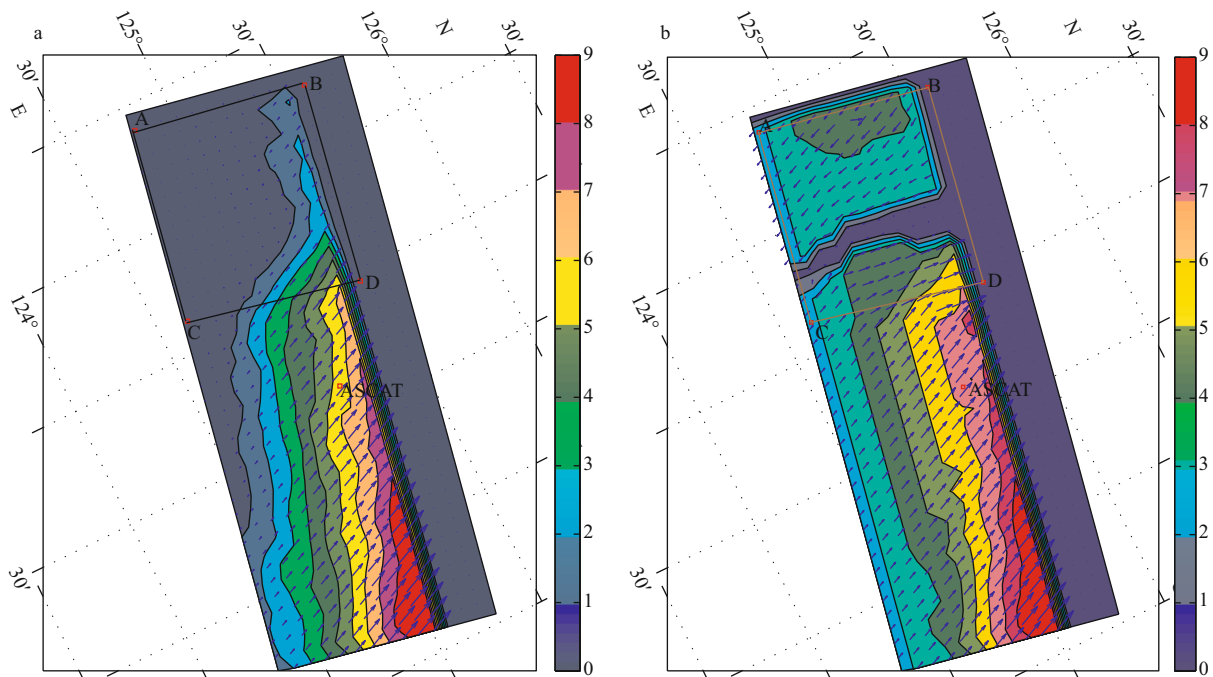
Fig.10 ASAR retrieved sea surface wind field in biogenic slicks area in East China Sea on July 20, 2011
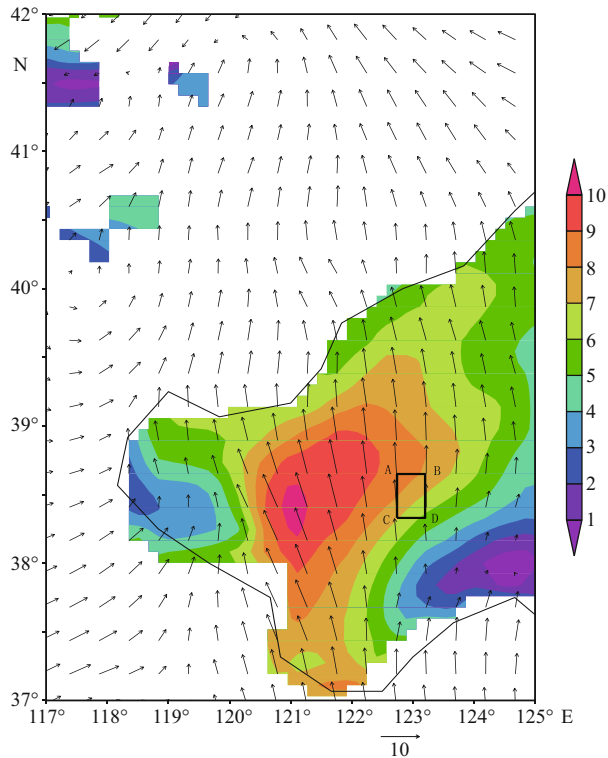a. wind field retrieved; b. wind field repaired (rectangle ABDC in Fig.3b).

Fig.11 Simulation in the WRF model for wind field at sea surface in the oil spill scene in the Bohai Sea at 10 AM on June 11, 2011 (rectangle ABDC in Fig.2b)

show that the RMS, A-error, and R-error in wind speed (wind direction) are 0.88 m/s (7.07°), 0.45 m/s (4.09°), and 0.01 m/s (-0.02°), respectively (Fig.14a, b). Please

notice that in Fig.10a, the initial wind speed at the red circle by the word ASCAT was about 5 m/s, which is obviously incorrect because of the influence by biogenic slicks and low wind zone. However, in Fig.10b, the wind speed was repaired to a correct one about 7 m/s, showing satisfactory repair reflected also in Fig.14a, b.

4 CONCLUSION

In this paper, we use the NRCS image samples of SAR to distinguish between the areas of oil spill, biogenic slicks, and clean sea, and using the adaptive threshold of NRCS to extract oil spill, biogenic slicks and to repair wind speed. The results obtained are good within the scope of the oil spill and biogenic slicks, demonstrating that this method can improve the accuracy of the assessment to the real wind field of an incident area. The attempt provides reference to medium and small scales wind field repair in oil spill and biogenic slicks and can contribute to the identification, surface monitoring of oil spills, biogenic slicks etc.
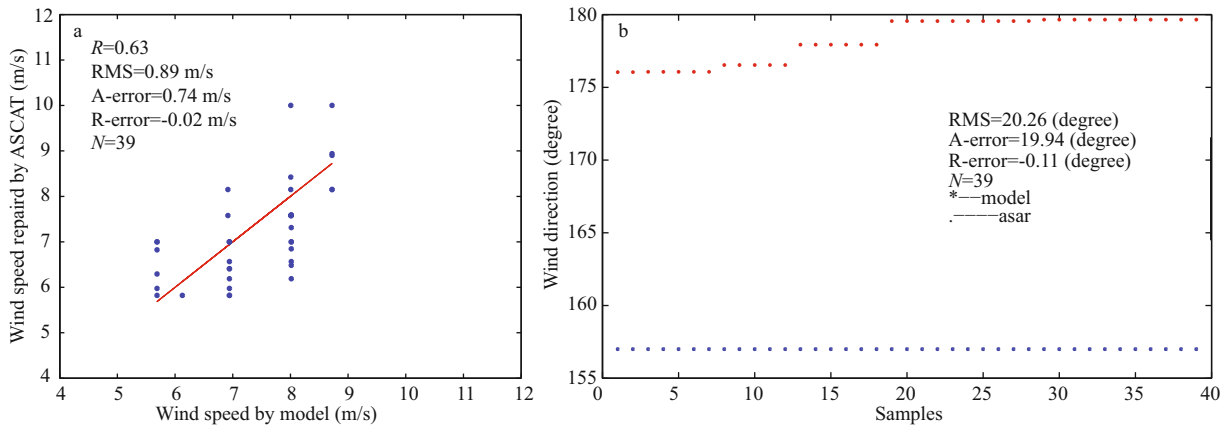
5 ACKNOWLEDGMENT

Fig.12 Comparison in wind speed (a) and wind direction (b) for the oil spill case on June 11, 2011 in the Bohai Sea between ASAR-retrieved and WRF-simulated results
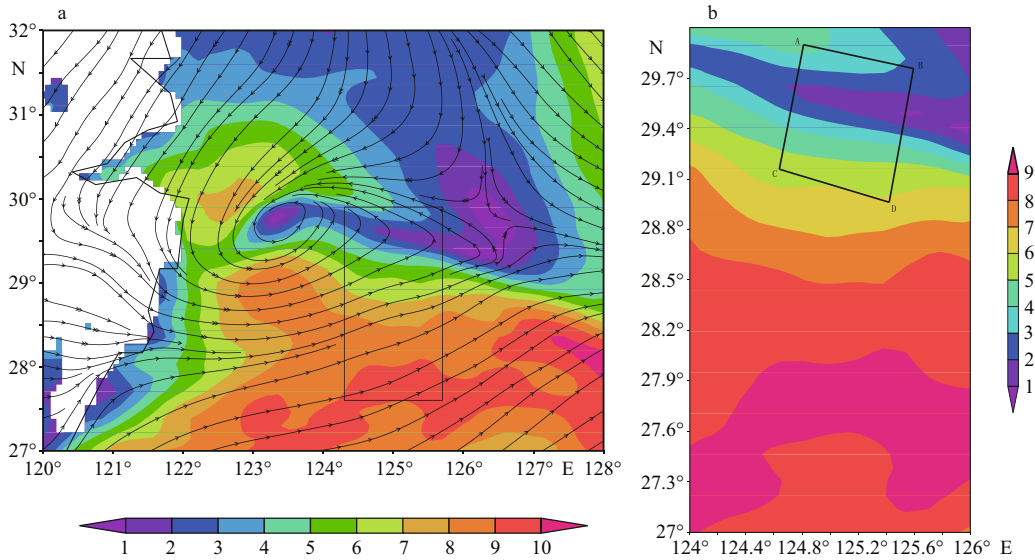

Fig.13 WRF-simulated sea surface wind field in biogenic slicks area of the East China Sea at 10 AM on July 20, 2011

The rectangle in Fig.13a shows the entire area of Fig.3a; Rectangle ABDC in Fig.13b covers the area the same as Fig.10b.
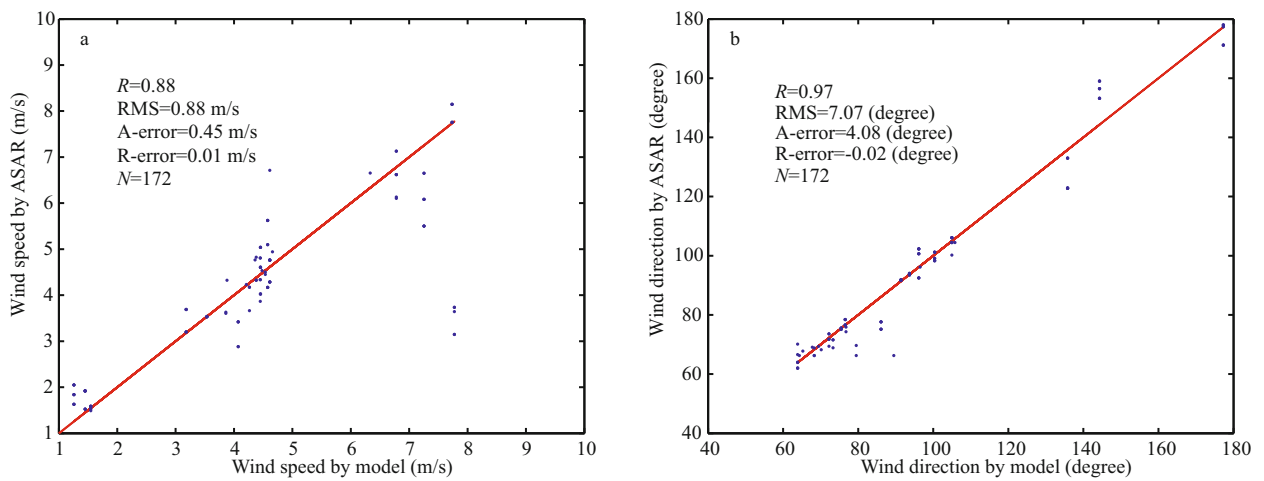

Fig.14 Comparison of wind speed (a) and wind direction (b) between WRF modeled and ASAR-retrieved for the scenario of July 20, 2011 in East China Sea

Table 2 Configuration of numerical simulation

Center coordinates	34°N, 124°E
Grid distance	18 km
Map projection	Lambert conformal conic
Grid size	121×121
Vertical levels	27
Time step	90 s
Microphysics	WSM 6-class Graupel scheme
Long wave radiation	RRTM scheme
Short wave radiation	Dudhia scheme
PBL physical	YSU scheme
Cumulus parameterization	Kain-Fritsch (New-Eta) scheme
Initial time	00Z10 June, 2011/00Z18 July, 2011
End time	12Z12 June, 2011/12Z20 July, 2011
History interval	60 s

References

Brekke C, Solberg A H S. 2005. Oil spill detection by satellite remote sensing. *Remote Sensing of Environment*, **95**: 1-13.

Del Frate F, Petrocchi A, Lichtenegger J, Calabresi G. 2000. Neural networks for oil spill detection using ERS SAR data. *IEEE Trans. Geosci. Remote Sens.*, **38**(5): 2 282-2 287.

Espedal H A, Johannessen J A. 2000. Detection of oil spills near offshore installations using synthetic aperture radar (SAR). *International Journal of Remote Sensing*, **11**: 2 141-2 144.

Espedal H A, Wahl T. 1999. Satellite SAR oil spill detection using wind history information. *International Journal of Remote Sensing*, **20**: 49-65.

Feng S Z, Li F Q, Li S Q. 2003. An Introduction to Marine Science. Higher Education Press. Beijing. p.242.

Fiscella B, Giancaspro A, Nirchio F, Pavese P, Trivero P. 2000. Oil spill detection using marine SAR images. *Int. J. Remote Sens.*, **21**(18): 3 561-3 566.

Gade M Alpers W. 1998. Imaging of biogenic and anthropogenic ocean surface films by the multifrequency/ multipolarization SIR-C/X-SAR. *Journal of Geophysical Research*, **103**(9): 18 851-18 866.

Guo J, Liu X, Xie Q. 2013. Characteristics of the Bohai Sea oil spill and its impact on the Bohai Sea ecosystem. *Chinese Science Bulletin*, **58**(19): 2 276-2 281.

Han J Q, Meng J M, Zhao J S. 2013. Feature extraction and its

criticality analysis for oil spill detection in synthetic aperture radar images. *Acta Oceanologica Sinica*, **35**(1): 85-93. (in Chinese with English abstract)

Hersbach H. 2010. Comparison of C-band scatterometer CMOD5.N equivalent neutral winds with ECMWF. *J. Atmos. Ocean. Technol.*, **27**(4): 721-736.

Karathanassi V, Topouzelis K, Pavlakis P, Rokos D. 2006. An object-oriented methodology to detect oil spills. *International Journal of Remote Sensing*, **27**: 5 235-5 251.

Keramitsoglou I, Cartalis C, Kiranoudis C. 2005. Automatic identification of oil spills on satellite images. *Environmental Modeling and Software*, **21**: 640-652.

Keramitsoglou I, Cartalis C, Kiranoudis C. 2006. Automatic identification of oil spills on satellite images. *Environ. Model. Softw.*, **21**(5): 640-652.

Migliaccio M, Nunziata F, Gambardella A. 2009. On the co-polarized phase difference for oil spill observation. *International Journal of Remote Sensing*, **30**(6): 1 587-1 602.

Quilfen Y, Chapron B, Elfouhaily T, Katsaros K, Tournadre J. 1998. Observation of tropical cyclones by high-resolution scatterometry. *J. Geophys. Res.*, **103**(C4): 7 767-7 788

Skamarock W C, Klemp J B. 2008. A time-split nonhydrostatic atmospheric model for weather research and forecasting applications. *J. Comput. Phys.*, **227**: 3 465-3 485.

Solberg A H S, Storvik G, Solberg R, Volden E. 1999. Automatic detection of oil spills in ERS SAR images. *IEEE Trans. Geosci. Remote Sens.*, **37**(4): 1 916-1 924.

Solberg R, Theophilopoulos N A. 1997. ENVISYS—A solution for automatic oil spill detection in the Mediterranean. Proceedings of 4th Thematic Conference on Remote Sensing for Marine and Coastal Environments. p.3-12.

Stoffelen A, Anderson D. 1997. Scatterometer data interpretation: Estimation and validation of the transfer function CMOD4. *J. Geophys. Res.*, **102**(C3): 5 767-5 780.

Topouzelis K, Karthanassi V, Pavlakis P, Rokos D. 2003. Oil spill detection: SAR multi-scale segmentation & object features evaluation. In Proceedings of SPIE. *Remote Sensing of the Ocean and Sea Ice*, **4880**: 77-87.

Topouzelis K, Stathakis D, Karathanassi V. 2009. Investigation of genetic algorithms contribution to feature selection for oil spill detection. *International Journal of Remote Sensing*, **30**(3): 611-625.

Zhang B, Perrie W, Vachon P W, Li X F, Pichel W G, Guo J, He Y J. 2012. Ocean vector winds retrieval from C-B and fully polarimetric SAR measurements. *IEEE Transactions on Geoscience and Remote Sensing*, **50**(11): 4 252-4 261.

Table 3 The root mean square error (RMS), absolute error (A-error), and relative error (R-error) of oil spill (as shown Fig.9b) and biogenic slick (in Fig.10b) (in rectangle ABDC) between WRF model data and SAR data

Date	Number	RMS-V (V_dir)	A-error-V (V_dir)	R-error-V (V_dir)
2011-06-11	39	0.89 m/s (20.26°)	0.74 m/s (19.94°)	-0.02 m/s (-0.11°)
2011-07-20	172	0.88 m/s (7.07°)	0.45 m/s (4.08°)	0.01 m/s (-0.02°)

$$\text{RMS} = \sqrt{\frac{1}{N}\sum_{k=1}^{N}(\omega_k^1 - \omega_k^2)^2} \; ; \; \text{A-error} = \frac{1}{N}\sum_{k=1}^{N}|\omega_k^1 - \omega_k^2| \; ; \; \text{R-error} = \frac{1}{N}\sum_{k=1}^{N}(\omega_k^1 - \omega_k^2)/\omega_k^2 \; ;$$ V: wind speed; V_dir: wind direction; N: number; ω: variable; k: 1:N